ChemCatChem

Research Article
doi.org/10.1002/cctc.202201670

Chemistry
Europe
European Chemical
Societies Publishing

www.chemcatchem.org

Effect of Metal Layer Support Structures on the Catalytic Activity of NiFe(oxy)hydroxide (LDH) for the OER in Alkaline Media

Christopher Gort[+],*[a] Paul W. Buchheister[+],[b] Malte Klingenhof,[b] Stephen D. Paul,[c] Fabio Dionigi,[b] Roel van de Krol,[d] Ulrike I. Kramm,[c] Wolfram Jaegermann,[a] Jan P. Hofmann,*[a] Peter Strasser,*[b] and Bernhard Kaiser[a]

Photoelectrochemical (PEC) cells promise to combine the benefits of photovoltaics and electrolysis in one device. They consist of a photoabsorber functionalized with an electrocatalyst to harvest faradaic currents under reduced overpotentials. To protect the absorber from the harsh reaction conditions, a protective buffer layer (e.g. TiO_2) is added between absorber and catalyst. In this work, we investigate the influence of the catalyst support systems Ti/TiO$_x$ and Ti/TiO$_x$/M (M = Au, Ni, Fe) on the overall activity and stability of nickel and iron mixed layered double hydroxides for the alkaline oxygen evolution reaction (OER). The catalyst performance on the bare Ti/TiO$_x$ substrate is very poor, but the incorporation of a metallic interlayer leads to two orders of magnitude higher OER current densities. While a similar effect has been observed for M = gold supported systems, we show that the same effect can be achieved with M = nickel/iron, already contained in the catalyst. This proprietary metal interlayer promises a cheap OER performance increase for PEC cells protected with titania buffer layers. Detailed XPS show an improved transformation of the starting catalyst material into the highly active (oxy)hydroxide phase, when using metallic interlayers. From these experiments a pure conductivity enhancement was excluded as possible explanation, but instead an additional change in the local atomic and electronic structure at the metal-support and metal-catalyst interfaces is proposed.

Introduction

Climate change together with dwindling fossil resources, are possibly the biggest challenges of our time. Therefore, the need for a sustainable future energy system is more vital than ever. Engineers and researchers around the world are implementing and improving renewable energy sources (RES) to manage our ever-growing demand for clean energy. Still, all renewable sources of electricity only work intermittently as they strongly depend on external variations, like tides, and the availability of sun or wind, which leads to a fluctuating electric power production. Therefore, the storage and supply of surplus energy from RES is of great importance. Hydrogen as a storage medium

is beneficial, because the only product when releasing the stored energy is pure water.[1,2] Furthermore, hydrogen can be used as feedstock in important industrial processes, among others in ammonia fertilizer- and steel production and possibly a wide range of hydrocarbon industries via methanation/Fischer–Tropsch processes.[3] Thus, hydrogen will certainly play an important role as an energy vector for a future zero emissions energy system.

The challenge however is to produce hydrogen on a large scale, in a cost-effective manner and without impacts on the environment. Renewable "green" hydrogen is primarily generated by electrolysis either in alkaline or acidic environment, but current production capacities are modest: in 2021, only 0.03%

[a] C. Gort,[+] Prof. W. Jaegermann, Prof. J. P. Hofmann, Dr. B. Kaiser
Department of Materials and Earth Sciences
Surface Science Laboratory
Technical University of Darmstadt
Otto-Berndt-Strasse 3
64287 Darmstadt (Germany)
E-mail: cgort@surface.tu-darmstadt.de
hofmann@surface.tu-darmstadt.de

[b] P. W. Buchheister,[+] M. Klingenhof, F. Dionigi, Prof. P. Strasser
Department for Chemistry
Technical Chemistry / Electrocatalysis
Technical University Berlin
Straße des 17. Juni 124
10623 Berlin (Germany)
E-mail: pstrasser@tu-berlin.de

[c] S. D. Paul, Prof. U. I. Kramm
Department for Chemistry
Catalysts and Electrocatalysts
Technical University of Darmstadt
Otto-Berndt-Strasse 3
64287 Darmstadt (Germany)

[d] Prof. R. van de Krol
Institute for Solar Fuels
Helmholtz-Zentrum Berlin für Materialien und Energie GmbH
Hahn-Meitner-Platz 1
14109 Berlin (Germany)

[+] These authors contributed equally to this work

Supporting information for this article is available on the WWW under https://doi.org/10.1002/cctc.202201670

ChemCatChem

Research Article
doi.org/10.1002/cctc.202201670

**Chemistry
Europe**
European Chemical
Societies Publishing

of the hydrogen produced was "green".[4] Catalysts to reduce overpotentials and increase efficiencies often include rare and expensive Pt-group metals and their oxides.[5] Recently, nickel iron layered double hydroxides (NiFe LDH) have extensively been studied as a cheap and promising catalyst material for the OER in alkaline electrolysis.[6–12] Linear sweep voltammetry (LSV) combined with differential electrochemical mass spectroscopy (DEMS) indicates that the catalyst undergoes oxidation from Ni^{2+} to Ni^{3+}, overlapping slightly with the onset of the oxygen evolution reaction (OER).[13] This oxidation leads to a reversible shortening of the interlayer distance, which is characteristic for the catalytically active species. Theoretical calculations have predicted that NiFe LDH undergoes a change from a α-Phase to an active γ-Phase, which was confirmed by *in-situ* WAXS measurements. The as prepared Nife LDH is non-conductive and only becomes conductive after the oxidation to the oxy-hydroxide.[6] While NiFe LDH shows a large OER activity on highly conductive materials (glassy carbon, stainless steel, nickel-felt), its activity on more stable, less conductive materials is of great interest for the implementation of NiFe LDH into advanced electrolysis cell stacks and photoelectrochemical (PEC) devices. Carbon anode supports are not suitable, due to carbon corrosion at potentials suitable for OER.[14–16] A common material used as a substrate for classical electrolysis is Ti with a native TiO_2 layer, due to its stability in even highly acidic or alkaline electrolytes. Since TiO_2 is a semiconductor with a wide band gap, it is further suitable as a protection layer for photoabsorbers in PEC applications. Incidentally TiO_2 was the first photoanode investigated for PEC.[17] Therefore, the interaction between cost effective and abundant titania materials as protection layer on one side and NiFe LDH as highly active co-catalyst on the other side is of great interest.[18,19]

Richter et al. recently studied the interaction of thin film metal catalyst layers of Ir, Ni and Au with amorphous TiO_2 surfaces. They observed, that the conduction behavior strongly depends on the band alignment at the interface and the corresponding work function differences between the TiO_2 layer and the metal film.[20] Besides that, investigations into the interaction between titania and transition metal oxides showed that nickel hydroxides have a dynamically changing interface when being polarized during OER.[21,22] Furthermore, the contact between transition metal nickel/iron oxide and hydroxide catalysts and their support layer (e.g. Ni, Fe, Cu, Ti, glassy carbon) has a strong influence on the observed OER activity in general.[23–27] All reports agree on the conducive effect of a metallic interlayer, for instance gold, boosting the observed activity by one to two orders of magnitude and this effect has been explained by both conductivity effects as well as changes in electronic properties of the catalyst. Nevertheless, a thorough understanding of this special behavior of Au or other metals is still missing.

In this work, we study the performance of state-of-the-art NiFe LDH prepared by deposition on different titania substrates with and without an additional metallic layer (Au, Ni, Fe) in-between. Depending on the used substrate, the OER activity does change quite drastically by several orders of magnitude. To gain a better understanding of this behavior, we compared dropcasted Ti/TiO_x/metal/NiFe LDH electrodes with thin film model systems of NiFe LDH, formed by reactive sputtering of thin layers of $NiFeO_x$ and subsequent electrochemical activation on the different substrates. From our experiments, we do not see that a reduced, more conductive titania plays a dominant role. Instead, we observe from our XPS studies, that the intermediate metallic layer improves the transformation of the initial nickel oxide/hydroxide to the more active phase considerably.

Results and Discussion

In the following we investigate different catalyst support systems on titanium substrates that have a native oxide layer on top. To keep the labeling consistent throughout this work we refer to the standard titanium substrate as Ti/TiO_x to highlight the sub stoichiometric nature of the native oxide layer (see Figure 3). The full devices are labelled Ti/TiO_x/M/Cat where M stands for the investigated metallic interlayers (Au, Ni, …) of which we mainly focus on nickel and gold and Cat stands for NiFe LDH or $NiFeO_x$ as a thin model system for the NiFe LDH catalyst. As far as possible, the system Ti/TiO_x/Au/Cat is color coded in red/orange shades in plots and the systems Ti/TiO_x/Cat without an interlayer and Ti/TiO_x/Ni/Cat with a nickel interlayer are kept in blue shades.

NiFe LDH catalysts by microwave-assisted synthesis

To understand the influence of the interaction of NiFe LDH with its support, we explored the OER performance under the use of different support materials by conducting LSV measurements. The synthesis for NiFe LDH follows a previously published and well established route, utilizing a microwave to form NiFe layered double hydroxide, showing low overpotentials for the OER, as well as in fuel cells as a bifunctional catalyst.[28–31] The catalyst loading was chosen as 0.2 mg/cm^2 following a previously published study on the ECSA of NiFe LDH, which showed that the OER activity reaches a plateau depending on the loading in RDE.[32] To circumvent loading based activity losses, we chose 0.2 mg/cm^2 which is firmly inside the plateau region. Although NiFe LDH has shown great promise as an OER catalyst on highly conductive support materials (glassy carbon), its activity towards the OER on Ti/TiO_x electrodes is close to zero (see Figure 1a). Even the implementation of a supposedly more conductive "leaky" TiO_2 as support material did not yield the desirable activity towards the OER.[33,34]

We conclude that titanium with a native oxide layer (Ti/TiO_x) is not suitable as a support layer for NiFe LDH without further treatment. Through the introduction of metal layers, sputter coated between the titanium substrate and the catalyst layer, we were able to improve the activity towards OER significantly. With sputtered gold layers (see Figure 1b)) – depending on the interlayer thickness – an activity comparable to or higher than that of NiFe LDH on glassy carbon (GC) could be achieved. Increasing the interlayer thickness to ca. 12 nm was sufficient to
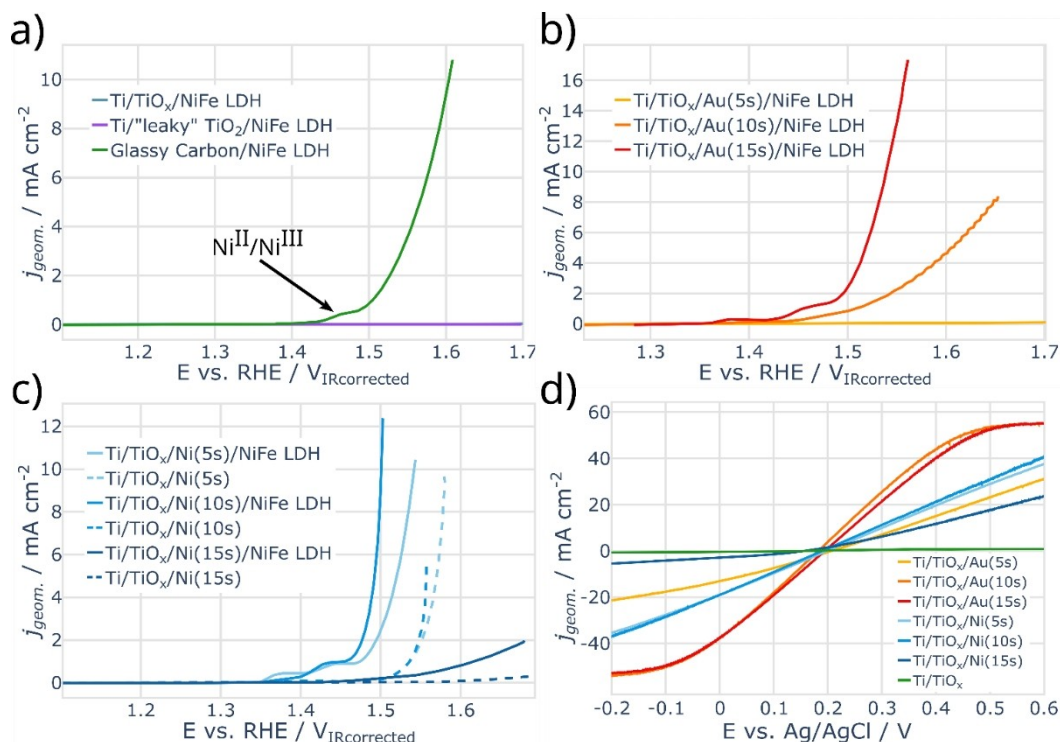
Figure 1. a) Linear sweep voltammetry (LSV) comparison of NiFe LDH OER activity on different titania supports and on glassy carbon. b) LSVs for NiFe LDH on different gold sputtered Ti/TiO_x supports. c) LSVs for NiFe LDH on different nickel sputtered Ti/TiO_x supports (solid) compared to the bare substrates without catalyst (dashed). The measurements were conducted at RT in 0.1 M KOH in a three-electrode setup. The catalyst loading was chosen as 0.2 mg/cm². SEM images of the titanium-based substrates from a) can be found in the SI (Figure S3l and S6l). d) LSVs of the catalyst free electrodes in a $K_4Fe(CN)_6/K_3Fe(CN)_6$ (0.01 M each) containing electrolyte (KCl 0.1 M) vs. a Ag/AgCl reference electrode.

produce highly active electrodes. The SI summarizes sputter time and thickness of the produced gold layer in Figure S3 and Table S1. We note that thicker gold interlayers (above 25 nm) tend to show a very unstable behavior when performing rotating disc electrode measurements. A more detailed analysis of the overall data indicates that for these samples already during the activation procedure, the current density dropped with each cycle, falling to half of the initial maximum value (see SI Figure S4). The mechanism of this deactivation is yet to be understood, but possibly includes a delamination of the catalyst or of the gold layers (see Figure S3l).

To mitigate this deactivation and offer a cost-efficient replacement for gold, nickel was tested as an interlayer material, yielding even slightly better activities and an enhanced stability during the activation routine (see Figure 1b), c) and S4). The sample with the intermediate thickness achieved the highest activity (see Figure 1c)). The reason for the observed thickness dependence has still to be clarified and requires more detailed interface growth experiments.

To further investigate the increase in activity by metal interlayers, experiments in an aqueous electrolyte containing a reagent that facilitates an outer-sphere redox-mechanism were conducted ($K_4Fe(CN)_6$ and $K_3Fe(CN)_6$ 0.01 M, each in 0.1 M KCl, see Figure 1d)). We were thus able to receive a reference point for the surface conductivity of the metal functionalized titanium substrates. The activities of the catalyst coated electrodes

towards OER follow the trend of the surface conductivity of the catalyst free electrodes. We note that the surface conductivity of the Au-coated electrodes is higher than that of the Ni-coated specimens, while catalyst coated samples with Au interlayers show less activity towards OER than the Ni coated ones. We contribute this to the activity towards OER of the nickel interlayer itself. In contrast to that, the blank Ti/TiO_x electrode passes almost no current. This indicates that the conductivity along the substrate-interlayer interface plays an important role in the investigated systems.

As shown, gold and nickel as interlayer materials yield comparable OER performances. To discriminate if either material has better stability properties, accelerated stress tests (AST, Figure 2b), d) and Figure S5) were performed with the as prepared electrodes. The AST consists of 2000 cyclic voltammetry (CV) measurements (1.1 V–1.6 V) with a holding time of 10 s at the beginning and the end of the sweeps. The catalyst and metal coated electrodes showed the expected behavior, with an increase in activity until a maximum is reached and a subsequent decline of activity, which was especially apparent in the gold coated titania electrodes. The NiFe LDH coated titania electrodes showed a stable but inactive behavior already after the first CV (see Figure S5), a fact which we attribute to the oxidation of the titanium species on the surface. The electrodes with both nickel and gold as an interlayer had an increase in maximum current density up until around 500 cycles. While the
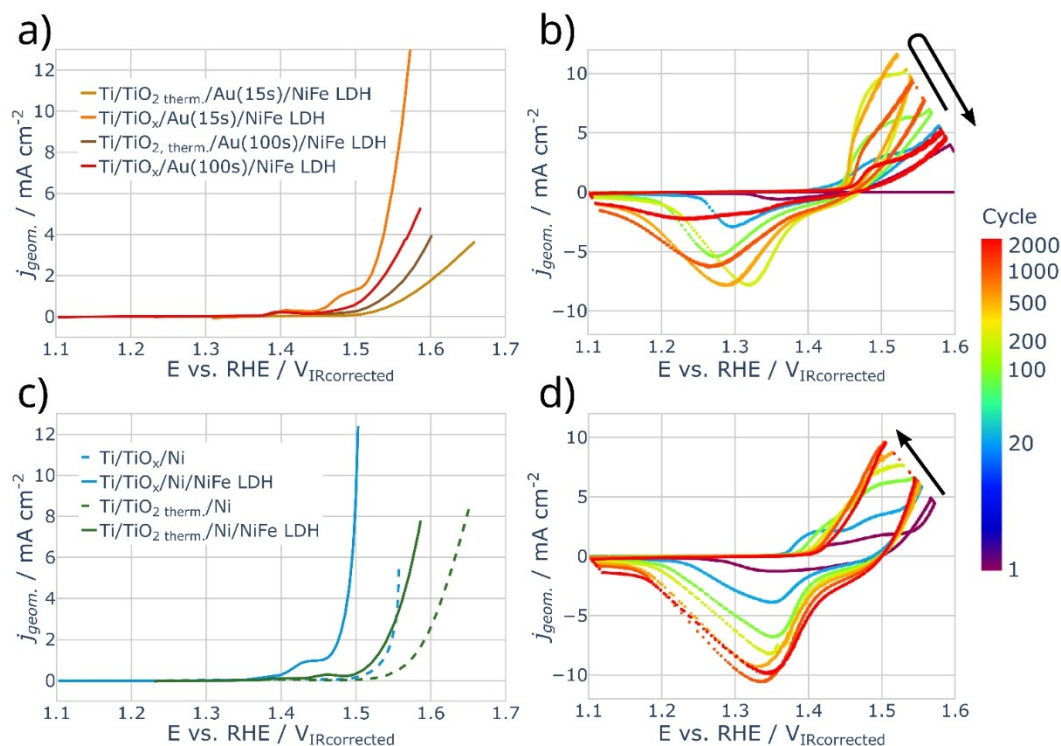
ChemCatChem

Research Article
doi.org/10.1002/cctc.202201670

Chemistry
Europe
European Chemical
Societies Publishing

Figure 2. a) and c) show the effect of thermal oxidation of the Ti/TiOx substrate before depositing the catalyst for gold and nickel as interlayers, respectively. In c), the dashed curves refer to a system with only the Ni interlayer and without the addition of the NiFe LDH catalyst layer. In b) and d) accelerated stress tests are shown to compare the stability of both interlayers (b) Ti/TiOx/Ni/NiFe LDH, d) Ti/TiOx/Au/NiFe LDH). The color scale to the right indicates the numbers of cycles that passed for each curve and is the same for both plots. The arrows indicate the trend of maximum current density with increasing cycles.

sample with a nickel interlayer stayed stable at this point, the sample with a gold interlayer showed a drop back to lower current density values. This again shows that nickel possibly possesses better adhesion properties to the Ti/TiOx, though the samples reach similar maximum current densities at one point.

To investigate if the direction of current flow has an effect on the investigated samples, we also studied them as cathodes for the HER. Here, we do not see the same increase in activity by addition of a gold interlayer (see SI Figure S7). The system Ti/TiOx/NiFe LDH already shows a good performance. Although the Ti/TiOx/Au/NiFe LDH electrodes still outperform the Ti/TiOx/ NiFe LDH electrodes, the major difference is only an earlier onset of the HER for samples with the gold interlayer. However, a strong contrast between NiFe LDH coated titania and blank titania electrodes is visible. While NiFe LDH barely improves the OER on titania compared to the blank electrodes, for the HER a distinct improvement is apparent. This indicates, that while electron transport from the catalyst to the titania electrode seems to be blocked, electron transport from the titania to the catalyst seems possible, thus forming a directional barrier for electron transport.[35] A possible explanation for this could be the formation of a Schottky contact between the titanium substrate and the metallic interlayer. Investigations of the electronic structure at the interface could elucidate this further, however are out of the scope of this work.

One possible explanation for the better OER performance of metal coated Ti/TiOx substrates could be that the metal layer

protects the conductive, sub stoichiometric titania surface layer from oxidation during OER.[20] To investigate the influence of these reduced Ti states, we performed experiments with titanium discs, that were pre-oxidized in an oven at 400 °C for 24 h in ambient atmosphere yielding substrates Ti/TiO$_{2, therm}$. The electrodes thus prepared were subsequently sputter coated with gold or nickel layers, drop-coated with NiFe LDH and investigated with regard to their OER activity. The treatment at 400 °C resulted in a thick layer of TiO$_2$ with barely any reduced Ti$^{2+/3+}$-states visible in the XPS-spectra (see Figure 3, green curve). The resulting LSVs are shown in Figure 2a) and c)). Although the observed activities are generally lower for the thermally oxidized, metal coated electrodes, they are still well above those of samples without metal interlayers, especially for samples with a nickel interlayer. Finally, electrochemical impedance measurements show similar high frequency resistances for the native Ti/TiOx samples, indicating similar conductivities (EIS, see Figure S8). In contrast, the low frequency region associated with charge transfer resistances is lower by about two orders of magnitude for metal coated titania electrodes. We conclude that the presence of reduced Ti species in the titanium oxide layer is not the main contribution to the improved activity of NiFe LDH on metal coated titania electrodes.
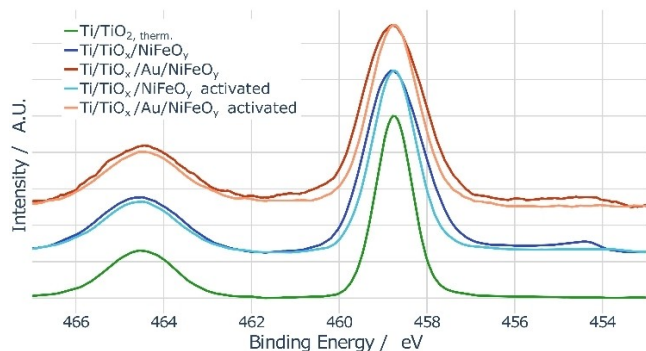
ChemCatChem

Research Article
doi.org/10.1002/cctc.202201670

Chemistry Europe
European Chemical
Societies Publishing

Figure 3. Ti 2p detail spectra for differently prepared samples: Ti/NiFeO$_x$ and Ti/Au/NiFeO$_x$ thin film systems as prepared (blue/red) and after electrochemical activation (light blue/orange). For reference a spectrum of a thermally oxidized Ti substrate without any catalyst layer (green) is shown. The binding energies were calibrated so that the Ti(IV)O$_2$ peaks are positioned at 458.7 eV.

NiFe oxide and hydroxide thin film catalysts by magnetron sputtering

To achieve a better understanding of the difference in the observed electrochemical activity of the layered systems, thin film nickel iron oxides were prepared on different substrates by magnetron sputtering. It has been shown that such thin films eventually turn into layered double (oxy-)hydroxide upon electrochemical conditioning and therefore represent well the properties of the NiFe LDH.[36] The prepared thin films were investigated with respect to their OER activity by LSV and their chemical composition and electronic structure using XPS. Figure S9 and S10 show cyclic voltammograms of the prepared thin film systems with and without different metallic interlayers, compared to the solvothermally prepared ones. Again, we observe a strong activity enhancing effect using a metallic interlayer between the Ti/TiO$_x$ substrate and the sputter deposited NiFeO$_x$ catalyst precursor. We can state that the preparation method has only a negligible influence, the dominant factor for device performance remains the inclusion of a metallic interlayer. For the XPS analysis we will focus on the system Ti/TiO$_x$/Au/NiFeO$_y$ as an example.

The layer thicknesses obtained from sputter deposition were controlled in such a way, that the information depth of the XPS is large enough to see all the way down to the Ti substrate, which enabled us to observe changes in the oxidation state of the Ti substrate, too. Ti 2p detail spectra are shown in Figure 3 for different thin film samples. The spectra were calibrated to the Ti 2p$_{3/2}$ peak of Ti(IV)oxide at 458.7 eV.[20,37] The thermally oxidized substrate (without catalyst on top) resembles best the a-TiO$_2$ core level spectrum from literature,[20,37] which shows characteristic peaks at $E_B = 458.7$ eV and $E_B = 464.5$ eV matching the Ti 2p$_{3/2}$ and 2p$_{1/2}$ peaks of Ti(IV)O$_2$. For the as-prepared catalyst samples, we observe a broadened TiO$_2$ signal due to the presence of crystal defect species and the substrate surface being sub stoichiometric and not fully oxidized. Additionally, we identify a metallic compo-

nent at $E_B = 454.3$ eV from the underlying substrate. After the electrochemical activation step, the metallic Ti signal vanishes, indicating further oxidation of the substrate and an increase in the thickness of the TiO$_2$ layer. This change is also clearly visible, if gold is used as an interlayer, showing that a thin gold layer is not able to protect the substrate below from oxidation. The electrochemical activation thus leads to an oxidation of the substrate to TiO$_2$ for all our thin film systems.

The oxidation is not as pronounced for the samples with gold, as visible from the broader *FWHM* of the peak at 458.7 eV resembling a more defect rich Ti(IV)O$_2$. The gold layer could help here in transportation of holes to the catalyst/liquid interface and thus avoid accumulation of oxidative hole species in the TiO$_x$ layer. This would protect reduced titania species from oxidation, or at least delay it, which would ensure that the TiO$_2$ layer remains conducting and able to provide charge carriers for the OER. Nevertheless, we can further pinpoint that suboxidised, defect rich titania phases do not play a major role in the observed performance increase by inclusion of a metallic interlayer.

Figure 4a) shows the Ni 2p$_{3/2}$ detail spectra for NiO (as reference) and the investigated NiFeO$_x$ thin films on Ti/TiO$_x$ and Ti/TiO$_x$/Au substrates. The latter show a similar shape of the main peak independent of the substrate used (w/ and w/o the Au interlayer). The Ni 2p spectra of NiO produced at identical conditions as our NiFeO$_x$ catalyst show a main peak at 853.7 eV
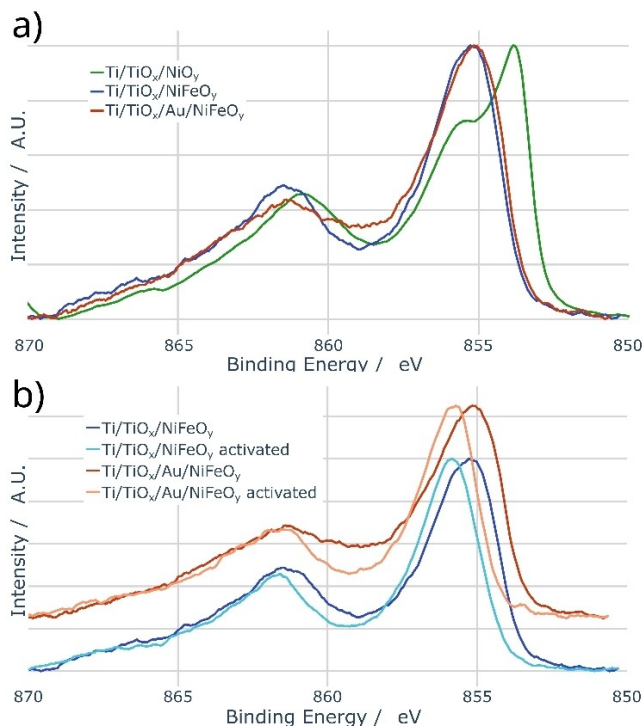

Figure 4. a) Ni 2p$_{3/2}$ detail spectra for pure nickel oxide (green) and mixed nickel-iron oxide on titania (blue) and titania+gold (red) substrates as prepared. b) Ni 2p detail spectra (calibrated to C 1s) of the systems Ti/TiO$_x$/NiFeO$_y$ (blue) and Ti/TiO$_x$/Au/NiFeO$_y$ (red) before (dark) and after electrochemical "activation" (light). Spectra were calibrated so that the C 1s peak from adventitious carbon coincides with 285.0 eV (see Figure S9).

ChemCatChem

Research Article
doi.org/10.1002/cctc.202201670

Chemistry Europe
European Chemical
Societies Publishing

with a shoulder at 855.5 eV and a satellite at around 860.8 eV, consistent with literature.[37–39] When switching to a NiFe alloy target for sputtering, the shoulder at 855.5 eV disappears and a broad peak remains. This main peak is centered at 855.3 eV for samples without a gold interlayer and shows a shift of 0.5 eV to lower binding energy when gold is introduced as an interlayer (see Figure S12). We attribute this shift to a changed energetic alignment to the substrate as we see the same shift in the O 1s spectra and the C 1s spectra of adventitious carbon. Therefore, all following spectra are calibrated to a binding energy of 285 eV for the C 1s peak of adventitious carbon (see Figure S11), if not mentioned otherwise. The position and shape of the Ni 2p3/2 main peak could hint to the presence of $Ni^{II}(OH)_2$ or even $Ni^{III}OOH$ in our pristine NiFeOx samples, as values between 855.0–855.6 eV have been reported in literature for these phases.[40–42]

However, the strong change in the shape of the main peak (Ni $2p_{3/2}$) has been attributed to a competition of screening electrons coming from the direct ligand shell and the electrons contributed by the neighboring transition metal ion (in our case Fe).[43] This peak shape change has also been observed recently for the case of mixed BiNi oxide thin films.[44] The spectra in Figure 4a) are therefore characteristic for NiFeOx. Figure 4b) shows the Ni 2p detail spectra for the $NiFeO_x$ samples before and after activation for the films with and without the gold interlayer. The main peaks are located at 855.3 eV and 855.2 eV for the untreated samples. The EC treatment leads in both cases to a blue shift of about 0.5 eV (independent of the red shift when introducing the gold interlayer with the same magnitude of 0.5 eV; shifts visible in Figure S12 but not all in Figure 4b) due to C 1s calibration). This is evidence for the formation of higher oxidized $NiFe(OH)_2$ or even NiFeOOH phases.[40,42,45,46]

Disregarding the energy shift, the peaks after electrochemical treatment overlap almost completely and represent an identical electronic configuration of Ni species. A similar observation is made for the solvothermally prepared samples, where the Ni 2p spectra possess the same shape independent of the used substrate (see Figure S14). We thus conclude that changing the underlying substrate does not affect the electronic structure of the Ni species in the $NiFeO_x$ catalyst by much.

Sensible Fe 2p spectra could not be obtained with our X-ray source, due to the Ni LMM Auger signal, which appears also at the respective binding energies. Furthermore, the lower cross section for the photoemission of Fe 2p electrons and the relatively low content of Fe in our samples gives only a weak signal that could not be separated from the Ni LMM Auger line for detailed interpretation.

The O 1s detail spectra for the different samples before and after electrochemical activation are shown in Figure 5. In the following we assign two components for each sample, which are separated by about 1 eV. These components are centered at around 530.1 eV with an *FWHM* of around 1.5 eV and at around 531.0 eV with a *FWHM* between 2.1–2.5 eV (for detailed fit parameters see Figure S13). The peak at lower binding energy can be assigned to lattice oxygen, whereas the high binding energy peak can be due to surface oxides and hydroxides.[39,40] From the fit of the two components, we see that the lattice oxygen species make up around 60% to 75% of the total O 1s intensity for samples with and without gold, respectively. The generally large *FWHM* is due to the contribution of the different metal oxides (Ni, Fe, Ti). Additionally, for the samples after electrochemical treatment, the intercalation of oxygen containing electrolyte constituents (e.g., H_2O) could give rise to a contribution at higher binding energies.

After the electrochemical activation process, we see a strong increase in the amount of OH^--like oxygen, which can be explained together with a slight blue shift of the emission (which has also been observed for the activated Ni 2p spectra (see SI Figure S12)) by the transformation of the surface oxide to the (layered double) hydroxide compound. This behavior is even more pronounced for the films with the gold interlayer.
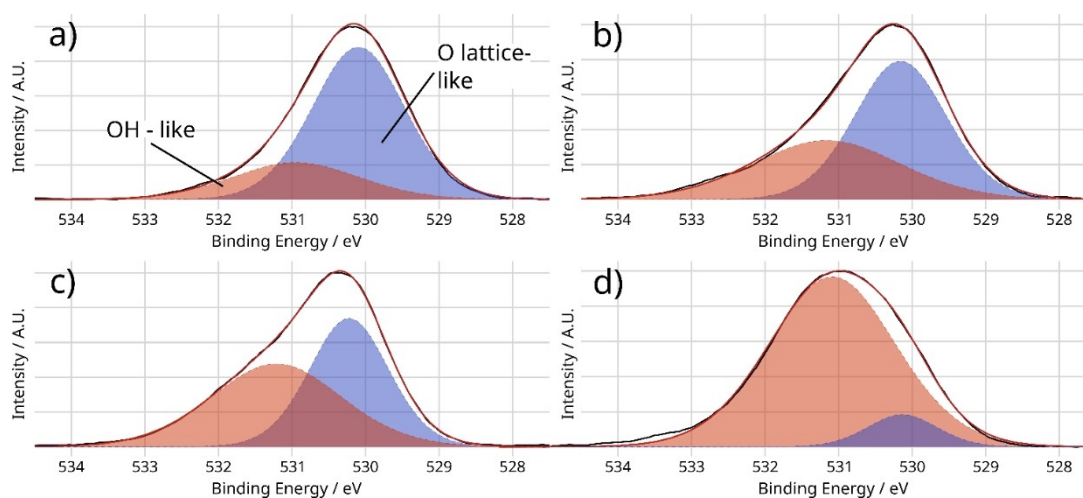

Figure 5. O 1s detail spectra (calibrated to C 1s) for a) $Ti/TiO_x/NiFeO_y$ before and c) after activation; b) $Ti/TiO_x/Au/NiFeO_y$ before and d) after activation. The black curves show the smoothed raw data, the blue solid area indicates lattice oxygen species and the red solid area surface oxide and hydroxide species. The red curve shows the fit envelope.

ChemCatChem

Research Article
doi.org/10.1002/cctc.202201670

Chemistry Europe
European Chemical
Societies Publishing

For the solvothermally prepared samples, we see the same behavior, with samples on Ti/TiO$_x$/Au substrates showing a much larger amount of higher binding energy oxygen species akin to oxy-/hydroxide species (see SI Figure S14). However, from the present measurements alone, we cannot discriminate in detail between the amount of double hydroxide or oxy-hydroxide and to which bonds these signals belong to.

To further investigate the source of the higher oxy-/hydroxide content, which seems to be correlated with higher OER performance, and to discriminate between a bulk or a surface effect, we prepared a series of samples with an increasing Au interlayer thickness and plotted the percentage of OH$^-$-like species against the layer thickness (see SI Figure S15). For the initial, not activated samples, the percentage of OH$^-$-like species increases from 25% to around 44% with increasing gold layer thickness. After electrochemical activation, the increase of OH$^-$-like species is even more sharp pronounced and the contribution of OH$^-$-like species increases from 50% to 90% within the first few metal monolayers, after which it reaches saturation between 1 and 1.5 nm thickness. This sharp increase after deposition of only a few monolayers of metal onto the TiO$_x$ substrate and the following saturation are evidence that the improvement in OER performance by metallic interlayers is rather a surface than a bulk effect. For thin film samples with a gold interlayer, we see an almost complete hydroxylation after electrochemical treatment of the initial NiFe metal oxide layer, which is not the case for the substrate without the Au layer. It is commonly known that sputter deposited gold films grow in islands for such thin layers, leaving in our case the substrate partially uncovered.[47,48] This indicates again that the metallic interlayer enhances the performance not by creating a thick buffer layer that protects the underlying Ti/TiO$_x$ from oxidation, but by promoting the transformation of the NiFeO$_x$ thin film into the more active (oxy)hydroxide. In contrast, samples where the catalyst (precursor) is directly deposited onto the Ti/TiO$_x$ substrate, only yield a partial transformation as visible from Figure 5 and a schematic of this is shown in Figure 6. It has been shown that NiFe LDH undergoes a transition under anodic potentials from an α-

Ni(OH)$_2$ like crystal phase to a γ-NiOOH like crystal phase.[6,27,49,50] Although there is an ongoing debate about which phase is the one promoting the OER under anodic polarization,[51,52] it has been observed from operando-XAS measurements that a γ-NiOOH like crystal phase is the active phase for NiFe LDH.[32,50,53] We therefore see reasons that the same effect leads to the observed performance increase in samples prepared in this work by both preparation methods.

Furthermore, we investigated also other metal substrate systems with XPS and electrochemical activity tests, i.e., iron (resulting in the system Ti/TiO$_x$/Fe/NiFeO$_y$). We see a similar OER performance increase as for gold and nickel, where the relative contribution to the O 1s of OH$^-$-like species starts at 28% and after activation increases to 67%. Choosing an adequate substrate thus enhances the conversion of the metal oxide/hydroxide species to the more active (oxy-)hydroxide species.

An enhancement of the OER activity of iron oxyhydroxides and nickel iron oxyhydroxides after introduction of Au and other metal interlayers has already been reported in previous studies, where the phenomenon has been explained in terms of a more homogenous deposition of the catalyst onto the Au surface, thereby yielding a film with good adhesion, low resistivity and a high number of active sites.[23–25] It has also been suggested that, a change in the local atomic and electronic structure might be another reason for the enhancing effect.[27,54–56] Therefore, we attribute the more complete transformation of the thin film catalyst precursors to (oxy-)hydroxides to the improved conductivity of the metallic interlayer, which provides enough charges for the hydroxylation of the precursor. This notion however does not hold for the samples that are solvothermally deposited directly on Ti/TiO$_x$, which show only a poor OER performance. These samples should be directly prepared as the OER active NiFe LDH phase and thus already be hydroxylated, needing no additional electrochemical activation (see the minimal changes in XPS before and after activation in SI Figure S14). The fact that we see here no change after electrochemical treatment could indicate that further phase transitions to the final OER active phase occur during anodic polarization only on metal function-
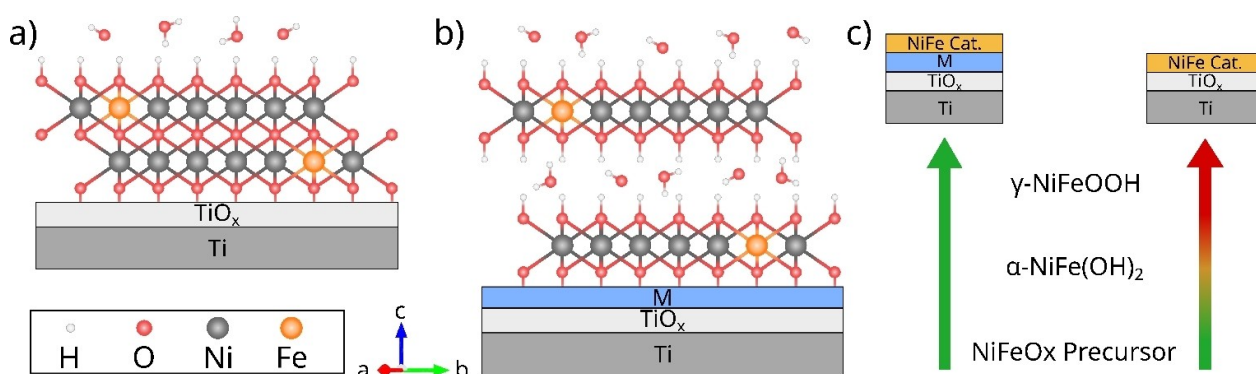

Figure 6. Different degrees of hydroxylation dependent on the substrate architecture. a) resembles partial activation as observed for samples Ti/TiO$_x$/NiFeO$_y$, b) shows a complete activation of the catalyst to a layered double hydroxide as assumed for the system Ti/TiO$_x$/M/NiFeO$_y$. c) The arrows in traffic light colors indicate how well the phase transition from the precursor to the γ–NiFeOOH is possible for the different used substrates. NiFe Cat. refers to either the solvothermal or the thin film samples investigated.

ChemCatChem

Research Article
doi.org/10.1002/cctc.202201670

Chemistry
Europe
European Chemical
Societies Publishing

alized titania substrates, which in turn can only be resolved with in operando techniques.

We suggest that besides electric conductivity, the morphology and the related electronic structure (Schottky contact, electronic level alignment in the substrate, interlayer, catalyst and electrolyte) between the catalyst and the substrate material as well as between the metal interlayer and the substrate play an important role for the finally observed improved activity for the samples with the metal interlayers. A thorough investigation of the influence of the different layers is required to obtain a full understanding of the decisive parameters. To achieve this goal, well-defined synthesis techniques coupled to in-situ and operando techniques are required for further investigations. Electronic structure calculations must accompany the experimental investigations.

Summary and Conclusions

In this work, we investigated the interaction of NiFe LDH OER catalysts and thin film NiFeO$_x$ catalyst precursors with different support systems consisting of Ti/TiO$_x$ substrates and various metal interlayers, e.g. Au, Ni and Fe. NiFe LDH catalysts, that were directly deposited on the Ti/TiO$_x$ substrate show only very poor activities. The addition of thin metal interlayers between the TiO$_x$ and the catalyst improves the OER activity by about two orders of magnitude. To understand this effect in more detail, we prepared thin film (1–2 nm) NiFeO$_x$ model systems by magnetron sputtering in UHV. These model films were tested with regard to their OER activity, showing in general a very similar behavior to the solvothermally prepared NiFe LDH. Using XPS, we studied the surface composition of the different systems directly after preparation, with different metal interlayers and after electrochemical activation. For all investigated samples, we observed that initially present conductive Ti^{3+}-rich titania phases were oxidized to Ti(IV)O$_2$ after electrochemical treatment and thus do not significantly affect the activity of the nickel based OER catalysts studied here, in contrast to the findings of Richter et al.[20] This becomes the more evident for the samples where we intentionally annealed the titanium substrates under ambient air to oxidize any defect species.

Obvious differences between the catalysts on samples with and without metal interlayers are observed in the O 1s XP spectrum, but not in the Ni 2p signal. We observe a broadening of the O 1s spectra, which is most likely due to the multi-component nature of our samples. Therefore, neither an exact composition nor the electronic structure can be unambiguously determined by XPS. From our investigations we interpret, that the metal interlayers lead to a faster and more complete transformation of the starting material to the catalytically more active or supportive hydroxide or oxyhydroxide phases yielding higher OER performances. Possible explanations for the observed OER activity increase could thus be a better energetic coupling between the substrate and the catalyst, mediated by the metallic interlayer. Though the exact mechanism for the increased activity by using a metallic interlayer stays elusive, we plan further investigations involving advanced operando characterization spectroscopies coupled with well-defined synthesis techniques.

We have shown that the successful extension of the metal interlayer concept from noble metals like gold to simple, abundant and cheap materials such as Fe and Ni can lead to an increase in overall efficiency and stability of (photo-)electrode/catalyst junctions. This offers a perspective for significant cost reductions in PEC systems for water splitting and could potentially lower the price for the green hydrogen that they produce.

Experimental Section

NiFe LDH preparation

NiFe LDH was synthesized in a solvothermal one-pot synthesis route using a microwave-assisted autoclave (Anton-Parr 300 Monowave). Prepared aqueous precursor solutions consisting of 1200 μL of 0.6 M Ni(OAc)$_2$·4 H$_2$O (Sigma Aldrich, 99.998% purity) and 240 μL of 0.6 M Fe(NO$_3$)$_3$·9 H$_2$O (Alfa Aesar, 98% purity) were added to 6 mL of dimethylformamide (DMF, Sigma Aldrich) and subsequently stirred for 12 h. After the initial crystallization, 8 mL of ultrapure water (>18 MΩ at room temperature) and 4 mL of additional DMF were added to the reaction mixture. The solution was then microwave-treated at 120 °C for 60 min and subsequently at 160 °C for 30 min. The final product was collected by centrifugation, then repetitively washed with ethanol and ultrapure water, and finally freeze-dried.

Titanium electrodes with a diameter of 10 mm were used for RDE measurements. The electrodes were polished with a polishing machine (Buehler eco-met 250) in three steps. For the first step, abrasive paper (Buehler carbimet SiC abrasive paper 400) was used with water as coolant and a polishing time of 10 min with a force of 25 N. After optical inspection for remaining scratches the polishing time could be increased. With the inspection passed, the electrodes were cleaned in deionized water in an ultrasonication bath 10 minutes and dried with pressurized nitrogen. In the second step, the electrodes were polished using a Nylon polishing cloth (Buehler Nylon polishing cloth) and 9 μm diamond suspension (Buehler MetaDi diamond suspension 9 μm) with a polishing time of 10 min and a force of 45 N. After optical inspection, the electrodes were cleaned again with deionized water in an ultrasonication bath and dried with pressurized nitrogen. The last polishing step was performed with a microcloth and 1 μm silica suspension (Buehler MasterMet 2) with a polishing time of 10 min and a force of 55 N. After cleaning in an ultrasonication bath and subsequent drying the electrodes could be used for the experiments.

A catalyst suspension/ink was prepared by dispersing 4 mg of NiFe LDH in 768 μL of Milli-Q-water, 200 μL of isopropanol and 32 μL of Nafion®-solution. The suspension was homogenized with a horn-sonifier for 15 min and used for drop-casting immediately afterwards. 40 μL of the prepared catalyst suspension was drop coated onto the precleaned and polished electrodes. Afterwards, the electrodes were dried at 50 °C for 10 minutes under atmospheric conditions. Some of the polished electrodes were sputter coated with gold, nickel or silver in Ar atmosphere (for metal film quality and thickness estimates see Figures S3 and S6). Furthermore, some electrodes were thermally oxidized under ambient air using a muffle furnace at 450 °C for 12 h. The so prepared electrodes were then coated with NiFe LDH as described above.

ChemCatChem

Research Article
doi.org/10.1002/cctc.202201670

**Chemistry
Europe**
European Chemical
Societies Publishing

Preparation of NiFeO$_x$ thin films

The substrate used for the thin film samples was Ti foil from Alfa Aesar (0.89 mm thickness, 99.7% metal basis). The Ti foil was cut into 1×1 cm^2 pieces and polished to mirror finish with 0.05 μm alumina MicroPolish (Buehler). After polishing, the samples were cleaned with soap before consecutively cleaning them 10 min in an ultrasonic bath first in isopropanol, then ethanol and finally blown dry with nitrogen. Depending on if the sample architecture included a gold layer, approx. 2 nm of gold (thickness estimation see experimental section on XPS) were deposited in a sputter coater (Quorum Technologies) onto the Ti substrates.

As the last step, thin films of NiFeO$_x$ were deposited by reactive radio frequency (RF) magnetron sputtering (MeiVac MAK 2″), using a metallic nickel/iron target (Kurt J. Lesker, 81%/19% mixture, 99.95% purity) in a gas mixture of 19.6 sccm argon (Air Liquide, 99.999%) and 0.4 sccm oxygen (Air Liquide, 99.995%) at a pressure of 1.5×10^{-2} mbar. The gas flow was regulated with mass flow controllers (MKS Instruments), and the RF power was set to 40 W. These metal oxide catalyst precursor films were then converted to layered double hydroxides via the electrochemical conditioning routine as described in the supporting information.

X-ray photoelectron spectroscopy

The chemical composition was investigated by X-ray photoelectron spectroscopy (XPS, SPECS) with a hemispherical energy analyzer (SPECS PHOIBOS 150) at a pressure $< 2 \times 10^{-9}$ mbar. As X-ray source, a monochromatized Al K$_\alpha$ source (1486.74 eV, SPECS Focus 500 with XR50M) was used. Survey spectra were recorded with a pass energy of 20 eV and a step width of 0.3 eV, detail spectra with 10 eV and 0.05 eV, respectively. The energy error of our device is estimated to be 0.05 eV, obtained from comparing different metal Fermi edges. Peak positions are however presented with an uncertainty of 0.1 eV due to complex spectra composition, especially for the shown Ni 2p detail spectra. Obtained spectra were analyzed by CasaXPS, version 2.3.22,[57,58] as well as in-house Python scripts, to employ Shirley background correction and Pseudo-Voigt peak fitting. The first step always consisted of linear Savitzky-Golay filtering to smooth plots and reduce noise. If not mentioned otherwise, the intensity axis for the XPS plots was min-to-max normalized, meaning the minimum value is set to zero and the maximal value to 1. For absolute intensity calculations relative sensitivity factors according to Scofield were used.[59]

To estimate the thickness of the deposited thin films, one side of the sample was masked during the deposition. In XPS, both sides were measured, and the thickness of the top layer was approximated by investigating how much the signal of the bottom layer was attenuated, i.e., how strong it is with and without the deposited layer on top. The deposited layer thickness can then be calculated by Equation (1):

$$d = \lambda \, ln\left(\frac{I_0}{I_s}\right) \qquad (1)$$

with λ being the mean free path of photoelectrons, I_0 the measured intensity of the bare substrate and I_s the intensity with the investigated layer on top. From this, it was estimated that the gold interlayer as well as the NiFeO$_x$ catalyst layer thicknesses for the thin film samples were 2 nm $\pm$ 1 nm.

Electrochemical analysis and catalyst activation

Electrochemical experiments on the NiFe LDH films were performed in a RDE setup with a Biologic SP-200 potentiostat. A platinum-mesh counter electrode was used next to a RHE reference electrode. Experiments were performed in a 0.1 M KOH solution, Milli-Q-water with a resistance above 18 MΩ cm was used to prepare the solutions.

Electrochemical measurements of the thin film systems were performed in a three-electrode cell (PECC-2, Zahner Elektrik GmbH) connected to a potentiostat (Interface 5000, Gamry instruments), using 0.1 M KOH (Carl Roth, 99.98%) as electrolyte. For reference Hg/HgO electrodes were used, which were calibrated against a SHE in 0.1 M KOH before usage. The counter electrode was a platinum wire. The employed measuring protocol includes an activation step, which consists of 20 cyclic voltammetry (CV) measurements performed at a scan rate of 50 mV/s in a potential range of 1.2 V to 1.6 V.

Conflict of Interest

The authors declare no conflict of interest.

Data Availability Statement

The data that support the findings of this study are available from the corresponding author upon reasonable request.

[1] R. Schlögl, *Chemical Energy Storage*, De Gruyter, Berlin, Boston **2022**.
[2] C. A. Grimes, S. Ranjan, O. K. Varghese (Eds.), *Light, Water, Hydrogen: The Solar Generation of Hydrogen by Water Photoelectrolysis*, Springer US, Boston, MA **2008**.
[3] V. Dieterich, A. Buttler, A. Hanel, H. Spliethoff, S. Fendt, *Energy Environ. Sci.* **2020**, *13*, 3207.
[4] Deloitte BE, *The potential of hydrogen in the chemical industry: White Paper* **2021**, https://www2.deloitte.com/content/dam/Deloitte/nl/Documents/energy-resources/POV-Hydrogen-Chemical-Industry-V12.pdf.
[5] *Iridium price | Umicore Precious Metals Management* **2022**, https://pmm.umicore.com/en/prices/iridium/.
[6] F. Dionigi, Z. Zeng, I. Sinev, T. Merzdorf, S. Deshpande, M. B. Lopez, S. Kunze, I. Zegkinoglou, H. Sarodnik, D. Fan, A. Bergmann, J. Drnec, J. F. de Araujo, M. Gliech, D. Teschner, J. Zhu, W.-X. Li, J. Greeley, B. R. Cuenya, P. Strasser, *Nat. Commun.* **2020**, *11*, 2522.
[7] F. Dionigi, P. Strasser, *Adv. Energy Mater.* **2016**, *6*, 1600621.
[8] F. Dionigi, J. Zhu, Z. Zeng, T. Merzdorf, H. Sarodnik, M. Gliech, L. Pan, W.-X. Li, J. Greeley, P. Strasser, *Angew. Chem.* **2021**, *133*, 14567.
[9] S. Dresp, F. Dionigi, M. Klingenhof, T. Merzdorf, H. Schmies, J. Drnec, A. Poulain, P. Strasser, *ACS Catal.* **2021**, *11*, 6800.

[10] B. M. Hunter, W. Hieringer, J. R. Winkler, H. B. Gray, A. M. Müller, *Energy Environ. Sci.* **2016**, *9*, 1734.

[11] X. Li, X. Hao, Z. Wang, A. Abudula, G. Guan, *J. Power Sources* **2017**, *347*, 193.

[12] H. Wang, K. H. L. Zhang, J. P. Hofmann, V. A. de La Peña O'Shea, F. E. Oropeza, *J. Mater. Chem. A* **2021**, *9*, 19465.

[13] R. L. Doyle, I. J. Godwin, M. P. Brandon, M. E. G. Lyons, *Phys. Chem. Chem. Phys.* **2013**, *15*, 13737.

[14] I. S. Filimonenkov, C. Bouillet, G. Kéranguéven, P. A. Simonov, G. A. Tsirlina, E. R. Savinova, *Electrochim. Acta* **2019**, *321*, 134657.

[15] S. Möller, S. Barwe, J. Masa, D. Wintrich, S. Seisel, H. Baltruschat, W. Schuhmann, *Angew. Chem. Int. Ed.* **2020**, *59*, 1585.

[16] Y. Yi, G. Weinberg, M. Prenzel, M. Greiner, S. Heumann, S. Becker, R. Schlögl, *Catal. Today* **2017**, *295*, 32.

[17] A. Fujishima, K. Honda, *Nature* **1972**, *238*, 37.

[18] K. Sivula, *ChemCatChem* **2014**, *6*, 2796.

[19] S. Hu, M. R. Shaner, J. A. Beardslee, M. Lichterman, B. S. Brunschwig, N. S. Lewis, *Science* **2014**, *344*, 1005.

[20] M. H. Richter, W.-H. Cheng, E. J. Crumlin, W. S. Drisdell, H. A. Atwater, D. Schmeißer, N. S. Lewis, B. S. Brunschwig, *Chem. Mater.* **2021**, *33*, 1265.

[21] F. Lin, S. W. Boettcher, *Nat. Mater.* **2014**, *13*, 81.

[22] F. A. L. Laskowski, M. R. Nellist, J. Qiu, S. W. Boettcher, *J. Am. Chem. Soc.* **2019**, *141*, 1394.

[23] J. W. D. Ng, M. García-Melchor, M. Bajdich, P. Chakthranont, C. Kirk, A. Vojvodic, T. F. Jaramillo, *Nat. Energy* **2016**, *1*, 1.

[24] P. Chakthranont, J. Kibsgaard, A. Gallo, J. Park, M. Mitani, D. Sokaras, T. Kroll, R. Sinclair, M. B. Mogensen, T. F. Jaramillo, *ACS Catal.* **2017**, *7*, 5399.

[25] L. J. Enman, A. E. Vise, M. Burke Stevens, S. W. Boettcher, *ChemPhysChem* **2019**, *20*, 3089.

[26] Z. Yin, R. He, Y. Zhang, L. Feng, X. Wu, T. Wågberg, G. Hu, *J. Energy Chem.* **2022**, *69*, 585.

[27] B. S. Yeo, A. T. Bell, *J. Phys. Chem. C* **2012**, *116*, 8394.

[28] S. Dresp, F. Luo, R. Schmack, S. Kühl, M. Gliech, P. Strasser, *Energy Environ. Sci.* **2016**, *9*, 2020.

[29] S. Dresp, P. Strasser, *ECS Trans.* **2016**, *75*, 1113.

[30] M. Gong, Y. Li, H. Wang, Y. Liang, J. Z. Wu, J. Zhou, J. Wang, T. Regier, F. Wei, H. Dai, *J. Am. Chem. Soc.* **2013**, *135*, 8452.

[31] M. Klingenhof, P. Hauke, S. Brückner, S. Dresp, E. Wolf, H. N. Nong, C. Spöri, T. Merzdorf, D. Bernsmeier, D. Teschner, R. Schlögl, P. Strasser, *ACS Energy Lett.* **2021**, *6*, 177.

[32] S. S. Jeon, P. W. Kang, M. Klingenhof, H. Lee, F. Dionigi, P. Strasser, *ACS Catal.* **2023**, *13*, 1186.

[33] Z. Guo, F. Ambrosio, A. Pasquarello, *J. Mater. Chem. A* **2018**, *6*, 11804.

[34] H. H. Pham, L.-W. Wang, *Phys. Chem. Chem. Phys.* **2015**, *17*, 541.

[35] X.-P. Li, W.-K. Han, K. Xiao, T. Ouyang, N. Li, F. Peng, Z.-Q. Liu, *Catal. Sci. Technol.* **2020**, *10*, 4184.

[36] M. S. Burke, L. J. Enman, A. S. Batchellor, S. Zou, S. W. Boettcher, *Chem. Mater.* **2015**, *27*, 7549.

[37] B. Vincent Crist, *Handbooks of Monochromatic XPS Spectra: Volume 2: Commercially Pure Binary Oxides* **2004**.

[38] H. Radinger, P. Connor, S. Tengeler, R. W. Stark, W. Jaegermann, B. Kaiser, *Chem. Mater.* **2021**, *33*, 8259.

[39] R. Poulain, J. Rohrer, Y. Hermans, C. Dietz, J. Brötz, J. Proost, M. Chatenet, A. Klein, *J. Phys. Chem. C* **2022**, *126*, 1303.

[40] B. P. Payne, M. C. Biesinger, N. S. McIntyre, *J. Electron Spectrosc. Relat. Phenom.* **2009**, *175*, 55.

[41] B. P. Payne, M. C. Biesinger, N. S. McIntyre, *J. Electron Spectrosc. Relat. Phenom.* **2012**, *185*, 159.

[42] S. Tao, Q. Wen, W. Jaegermann, B. Kaiser, *ACS Catal.* **2022**, *12*, 1508.

[43] M. A. van Veenendaal, G. A. Sawatzky, *Phys. Rev. Lett.* **1993**, *70*, 2459.

[44] J. Morasch, *Deposition, Charakterisierung und Bandanpassung oxidischer Dünnschichtmaterialien zur Lichtabsorption*, Darmstadt **2017**.

[45] A. P. Grosvenor, M. C. Biesinger, R. S. Smart, N. S. McIntyre, *Surf. Sci.* **2006**, *600*, 1771.

[46] M. C. Biesinger, B. P. Payne, L. W. M. Lau, A. Gerson, R. C. St. Smart, *Surf. Interface Anal.* **2009**, *41*, 324.

[47] M. Schwartzkopf, A. Buffet, V. Körstgens, E. Metwalli, K. Schlage, G. Benecke, J. Perlich, M. Rawolle, A. Rothkirch, B. Heidmann, G. Herzog, P. Müller-Buschbaum, R. Röhlsberger, N. Stribeck, S. V. Roth, *Nanoscale* **2013**, *5*, 5053.

[48] L. Armelao, D. Barreca, G. Bottaro, A. Gasparotto, M. Losurdo, E. Tondello, *Mater. Sci. Eng. C* **2005**, *25*, 599.

[49] L. Trotochaud, J. K. Ranney, K. N. Williams, S. W. Boettcher, *J. Am. Chem. Soc.* **2012**, *134*, 17253.

[50] D. K. Bediako, B. Lassalle-Kaiser, Y. Surendranath, J. Yano, V. K. Yachandra, D. G. Nocera, *J. Am. Chem. Soc.* **2012**, *134*, 6801.

[51] P. W. T. Lu, S. Srinivasan, *J. Electrochem. Soc.* **1978**, *125*, 1416.

[52] Y.-F. Li, J.-L. Li, Z.-P. Liu, *J. Phys. Chem. C* **2021**, *125*, 27033.

[53] D. Friebel, M. W. Louie, M. Bajdich, K. E. Sanwald, Y. Cai, A. M. Wise, M.-J. Cheng, D. Sokaras, T.-C. Weng, R. Alonso-Mori, R. C. Davis, J. R. Bargar, J. K. Nørskov, A. Nilsson, A. T. Bell, *J. Am. Chem. Soc.* **2015**, *137*, 1305.

[54] J. Zhang, J. Liu, L. Xi, Y. Yu, N. Chen, S. Sun, W. Wang, K. M. Lange, B. Zhang, *J. Am. Chem. Soc.* **2018**, *140*, 3876.

[55] W. Zhu, L. Liu, Z. Yue, W. Zhang, X. Yue, J. Wang, S. Yu, L. Wang, J. Wang, *ACS Appl. Mater. Interfaces* **2017**, *9*, 19807.

[56] H. Gu, G. Shi, H.-C. Chen, S. Xie, Y. Li, H. Tong, C. Yang, C. Zhu, J. T. Mefford, H. Xia, W. C. Chueh, H. M. Chen, L. Zhang, *ACS Energy Lett.* **2020**, *5*, 3185.

[57] Alan Carrick, *The casa cookbook* **2005**.

[58] N. Fairley, V. Fernandez, M. Richard-Plouet, C. Guillot-Deudon, J. Walton, E. Smith, D. Flahaut, M. Greiner, M. Biesinger, S. Tougaard, D. Morgan, J. Baltrusaitis, *Appl. Surf. Sci. Adv.* **2021**, *5*, 100112.

[59] J. H. Scofield, *J. Electron Spectrosc. Relat. Phenom.* **1976**, *8*, 129.